Università Politecnica delle Marche

Department of Information Engineering (DII)

Master of Science in Biomedical Engineering

Near-Field Inverted Scanning Microwave Microscopy

Author:

Siti Nur Afifa binti Azman

Supervisor:

Prof. Marco Farina

Co-advisor:

Dr. Eleonora Pavoni

October 2020

Academic Year 2019/2020

Acknowledgment

First and foremost, I would like to express my sincere appreciation to my supervisor, Professor Marco Farina, whose expertise was invaluable, providing me the opportunity to learn from his exceptional scientific knowledge. It was a real privilege and an honor for me to complete my thesis under his supervision.

I would also like to extend my deepest gratitude to my co-advisor, Dr. Eleonora Pavoni, for her constant support, availability, and constructive suggestions, which were determinant for the accomplishment of the work presented in this thesis.

Special thanks to Dr. C. H. Joseph and Gianluca Fabi for valuable guidance, encouragement, and assistance despite their busy schedule, which has helped me develop and improve my skills.

I am extremely grateful to my parents for their love, prayers, caring and sacrifices for educating and preparing me for my future. To my siblings for always believing in me and encouraging me to follow my dreams, thank you.

Finally, many thanks to all my friends who directly or indirectly helped me to complete this thesis.

Contents

Abstract

Near-field Scanning Microwave Microscopy (NSMM) is a technique that produces an image from the evanescent microwave field interacting with the sample with the spatial resolution down to the atomic scale. This technique is commonly used simultaneously with any scanning probe microscopy (SPM) technique, such as the atomic force microscopy (AFM) or the scanning tunneling microscopy (STM). The NSMM is prominent for providing non-invasive imaging of sub-surface structures and allowing local quantitative characterization of the sample. Regardless, a novel technique known as near-field Inverted Scanning Microwave Microscopy (iSMM) is the improvement developed recently to broaden the application beyond the current focus on surface physics and semiconductor technology. Despite the iSMM offer advantages over NSMM, this technique has not been widely commercialized and the system setup needs to be custom designed according to the existing instruments we have in our microscopy laboratory. In the present work, the iSMM setup was constructed with a slight modification of SPM probe into a simple and rugged metal tip, and utilization of a transmission line as part of the sample holder. The setup was then evaluated by performing the sensitivity test, waveguide analysis and verified by scanning on real sample. The microwave image (S_{11}) of graphite at frequency 12.03 GHz acquired by the AFM-modified iSMM. After applying proper calibration procedure and the time domain analysis, the quality of the iSMM image is improved and the details of graphite flake is well visible. The AFM-modified iSMM has been successfully developed for real sample analysis at high frequencies.

Chapter 1

General Introduction

1.1 Overview of Scanning Probe Microscopy

Scanning Probe Microscopy (SPM) is a powerful metrology tool that has been a major breakthrough in nanotechnology, providing access to visualize and study sample properties at the atomic level. The working principle of SPM is utilizing a sharp probe to perform a raster scan in close proximity to the sample surface and recording the tip-sample local interaction signal. The feedback system is employed to maintain the interaction by adjusting the tip-sample position height so that the tip-sample separation can be controlled during the scanning process. The adjustment of the tip position performed by the piezo scanner in three dimensions with the sub-nanometer resolution is monitored thereby producing the atomic-scale resolution topographic image. Various types of interaction are exploited in different types of SPM techniques, chosen according to the characteristics of the sample and the purpose of the study. Figure 1.1 shows the generalized schematic diagram of SPM.

Besides, the SPM techniques are able to perform in different kinds of environments like ultra-high vacuum [1] [2], air [3] [4], and liquid [5] [6]. Scanning Tunneling Microscopy (STM) is the first SPM technique invented by G. Binnig and H. Rohrer in 1981 [7] then were awarded the Nobel Prize in physics in 1986. However, it re-

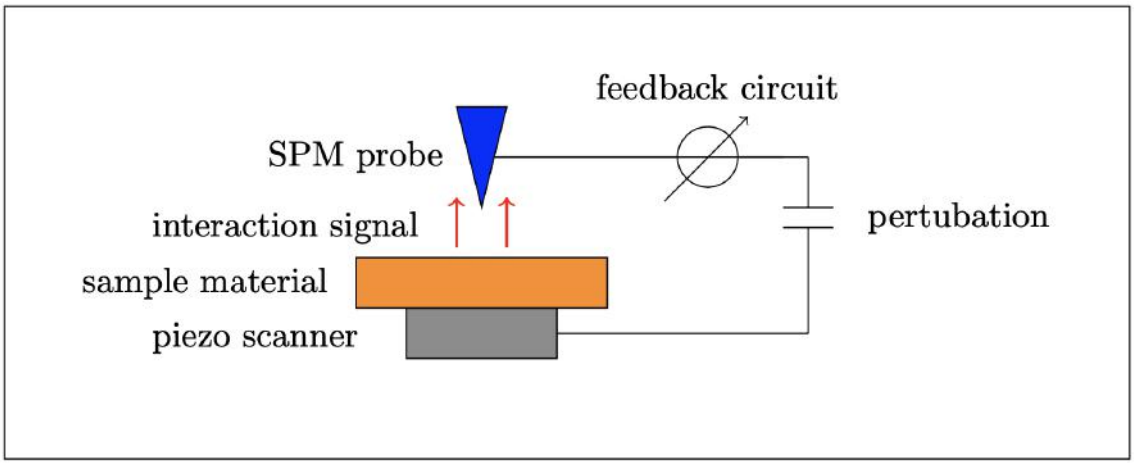

Figure 1.1: The generalized schematic diagram of SPM

quires a conducting and semi-conducting sample surface. This main limitation has led to the invention of Atomic Force Microscopy (AFM) [8] that broadens the application to a wide variety of samples. Both STM and AFM techniques will be further discussed in the next sections respectively.

1.1.1 Scanning Tunneling Microscopy

The STM working principle is based on the quantum-mechanical phenomenon of tunneling current. As the tip approaches the conductive or semi-conductive sample surface to distances of few nanometers (nm), the tunnel current is produced as a consequence of the bias applied between the tip and the sample causing the electrons to flow through the narrow potential barrier [9]. In this way, the distance between the tip and the sample surface is maintained thanks to the exponential decay of the tunnel current over the tip-sample distance. Figure 1.2 shows the basic principle of STM.

Generally, the STM can operate either in constant current mode or constant height mode. In constant current mode, the STM feedback system is used to keep the tunnel current constant by adjusting the tip height at each measurement point over the sample. For example, when the system detects an increase of tunnel current,

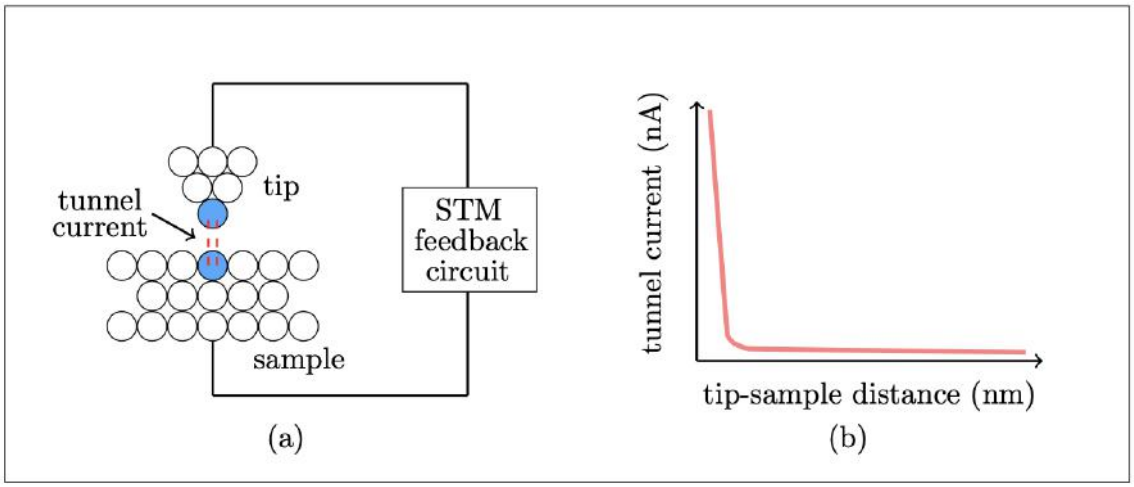

Figure 1.2: (a) The STM feedback system and (b) the relationship between the tunnel current and the tip-sample distance

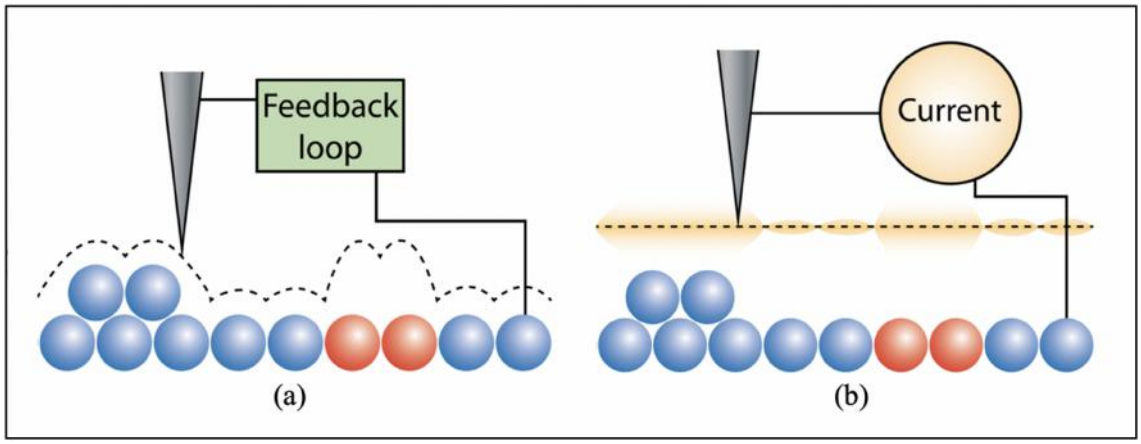

Figure 1.3: The STM modes and the dotted line indicates the path following by the STM probe tip. (a) The constant-current mode. The red atoms exhibit different height paths compare to the blue atoms due to differences in the local density of states. (b) The constant height mode. The orange glow along a constant height path represents the recorded tunnel current. The glowing is more for the higher tunnel current detected than the surrounding surface

it adjusts the voltage applied to the piezo scanner to increase the distance between the tip and the sample, refer Figure 1.3 (a). The tip height variation measurements are then used to produce the STM topographic image. In constant height mode instead, the feedback system can be turned off as the tip is scanned at a constant height. The changes in tunnel current due to the sample topography and local density states are measured at each point, refer Figure 1.3 (b). Such measurements are used to produce the STM image. This mode is faster as no displacement of

tip height involves, but it provides useful information only for relatively smooth surfaces.

Apart from the limitation of STM to conductive and semi-conductive samples, it also requires high bias especially for the dielectric samples to allow current tunneling which can cause overheating to the instrument. Therefore, AFM is a good alternative and more preferable by many research groups.

1.1.2 Atomic Force Microscopy

The AFM probe comprises of a sharp tip mounted on the flexible cantilever and the working principle is based on the optical beam bounce approach. This approach involves the reflected laser beam on the cantilever serves as a means to measure the interaction forces between the tip and sample. As the tip approaches the sample surface to distances of several nanometers (nm), the deflection of the cantilever due to the detection of the atomic forces is translated into an electrical signal corresponding to the motion of the reflected laser beam on the photodetector. The intensity of the electrical signal is proportional to the cantilever deflection.

In the AFM technique, there are several forces involved, called Van der Waals force, which originated from intramolecular interaction. When the tip is brought extremely close to the sample, the repulsive force dominates while as the tip is retracted from the sample, the attractive force quickly becomes dominant. Nevertheless, the tip-sample distance has to be close enough to be able to detect such forces.

The AFM has three operation modes contact, non-contact, and tapping modes. In contact mode, the tip is scanned in direct contact with the sample surface. Meanwhile, in non-contact and tapping modes, the cantilever oscillates at the resonant frequency throughout the scanning process. The tapping mode is usually employed to enhance the AFM sensitivity as it reduces the tip pressure applied to the sample

at which it becomes relevant especially for soft biological samples. Figure 1.4 shows the basic principle of AFM.

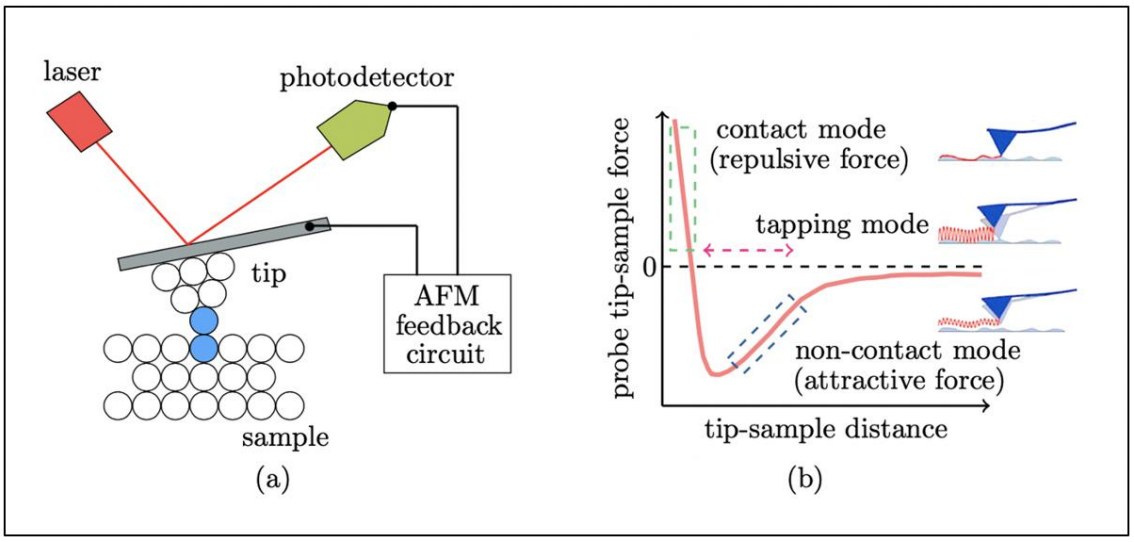

Figure 1.4: (a) The AFM feedback system and (b) the relationship between tip-sample force and the tip-sample distance

The AFM feedback system monitors the reflected laser beam to keep the interaction forces constant by adjusting the tip-sample distance, performed by the piezo scanner. In contact mode, the forces are kept constant by maintaining the cantilever deflection whereas, in non-contact and tapping modes, the amplitude of the oscillation is maintained. The variation of tip height is recorded and is used to produce the AFM topographic image.

1.1.3 Near-Field Scanning Microwave Microscopy

Near-field Scanning Microwave Microscopy (NSMM) is a technique that integrates a microwave signal path into SPM to study the local electromagnetic properties response of the sample through its interaction with the scanning probe, in contact or non-contact at near-field within nanometer (nm) scale, known as the evanescent field. In such a manner, high spatial resolution down to atomic scale can be achieved, resolving the resolution limitation in classical optical principle, the Abbe's limit [10]. The basic components of NSMM consist of a microwave source, a scanning probe, a

detector system as shown in Figure 1.5 below.

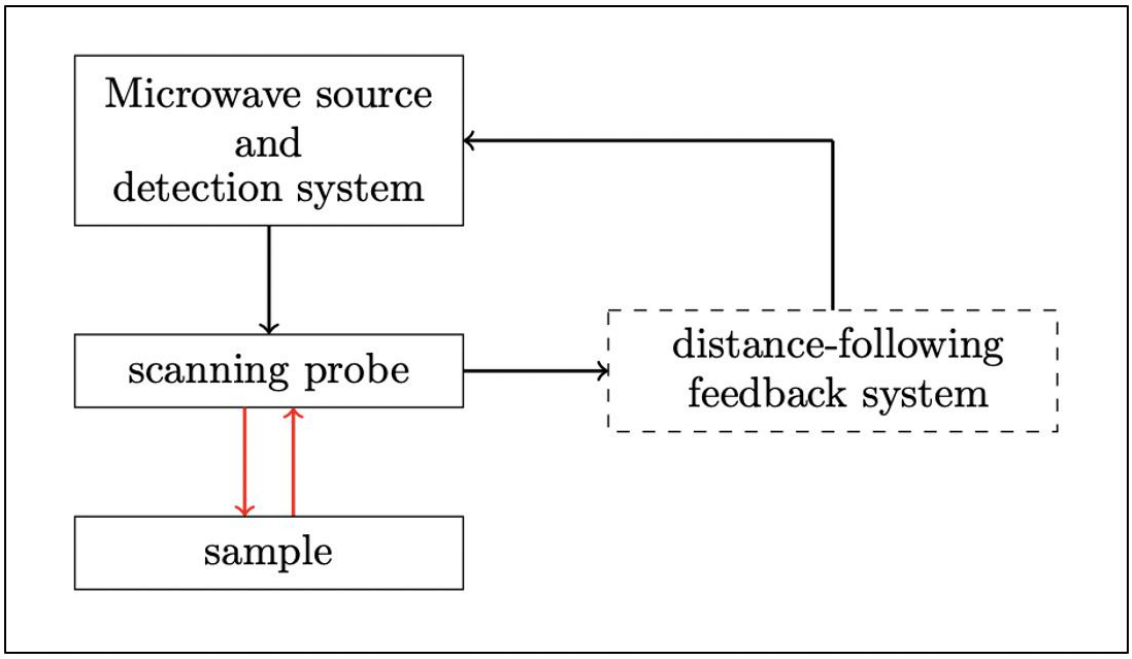

Figure 1.5: The SMM basic schematic diagram

Usually, the vector network analyzer (VNA) is employed as both the microwave source and the detection system. As the detection system, the VNA provides the microwave response measurement in terms of the reflection and transmission coefficients describe in S-parameters. These parameters are in a complex form composed of magnitude and phase characteristics of the signal. The reflection coefficients (S_{11} and S_{22}) involves a one-port configuration measurement and are defined as the ratio of the reflected signal to the incident signal. The transmission coefficients (S_{21} and S_{12}), on the other hand, involves two-port configurations measurement, defined as the ratio of the transmitted signal to the incident signal. Figure 1.6 shows the S-parameters of VNA in the two-port network, commonly study in NSMM.

The scanning probe of NSMM is utilized as an antenna and a receiver to transmit and detect the signal separately. The probe can be aperture-based or apertureless. The aperture-based probe has an open-ended aperture such that the incident and reflected signals only confined to the local region, but causes high signal attenuation as the incident signal will have to pass the cut-off region. Thus, the apertureless

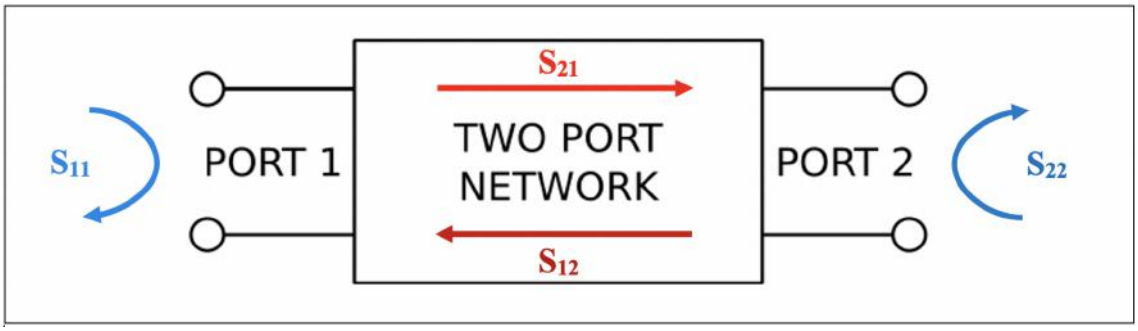

Figure 1.6: The S-parameters of VNA in two-port network

probe is currently predominant and it uses a sharp tip to allow the field-concentrating feature to intensify the incident signal locally.

The main idea of NSMM is the use of the probe tip to scan in contact or in close proximity to the sample surface at a distance, d typically less than one-tenth of tip dimensions, D, establishing a high signal-to-noise ratio (SNR) [11], refer Figure 1.7.

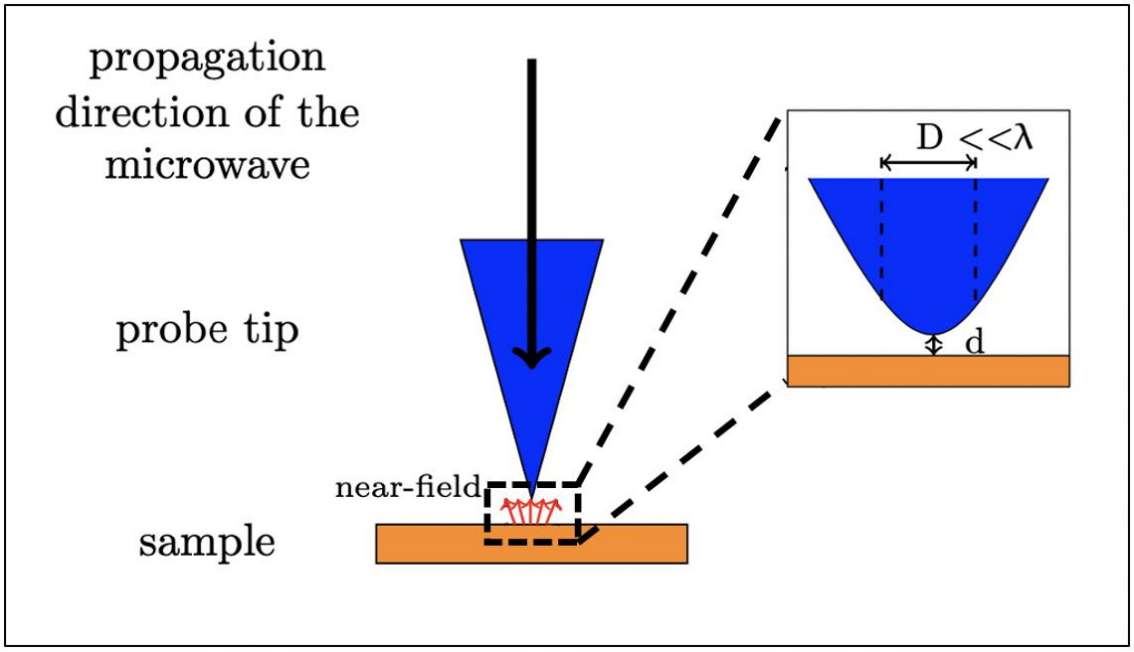

Figure 1.7: The near-field apertureless probe

As the NSMM records the interaction signal in the evanescent field that is concentrated in the vicinity of the tip apex, the tip-sample distance has to be maintained during the scanning process to ensure the high precision of the near-field measurement. Therefore, the evanescent waves are responsible for the imaging capabilities of

the NSMM and the spatial resolution is determined by the tip apex dimensions [11]. The short distance between the tip and the sample can be maintained by exploiting the STM or the AFM feedback circuit in the NSMM distance-following system due to the fact both techniques share the operating principle that able to control the tip-sample distance with atomic-scale precision. The integration of NSMM with the STM (STM-based SMM) or AFM (AFM-based SMM) allows acquiring electromagnetic properties and topographic images simultaneously.

The NSMM can be either resonant or non-resonant based on the system setup and the microwave response can be presented in different manners such as resonant frequency, f and quality factor, Q in resonator-based microscopy, or reflection coefficient, Γ and transmission coefficient, T for both real and imaginary parts in other cases.

For a resonant microscope, a resonator is introduced in the system that is coupled to the microwave source at one end and connected to the probe at the other end. It operates at a resonant frequency and involves monitoring the reflection or transmission properties at a point of maximum slope of the response curve. The changes in resonant frequency, Δf, and quality factor, Q represent the microwave response of the sample are measured, refer Figure 1.8 (a). By having a resonator in the NSMM, the sensitivity of the system increases but it is restricted to narrow-band frequency. Therefore, a resonant microscope is efficient only for which frequency it was designed.

For a non-resonant or broadband microscope, a transmission line, either coaxial or waveguide, is used as a signal path from the microwave source to the probe. This physical implementation involves cable connections, adapters, and the transition from the guided-wave structure to the probe. As a consequence, multiple minima are generated in the magnitude of the reflection coefficient corresponding to the cumulative effect of the interfaces and associated impedance mismatch. Thus, a

fixed or a frequency range has to be selected for the operating frequencies of the NSMM to maximize the SNR, which is often found by trial and error. Then, the microwave response of the sample, the reflection coefficient, Γ and/or transmission coefficient, T for both real and imaginary parts are obtained, refer Figure 1.8 (b). By having a broadband system in NSMM, it opens the possibility to perform local microwave spectroscopy.

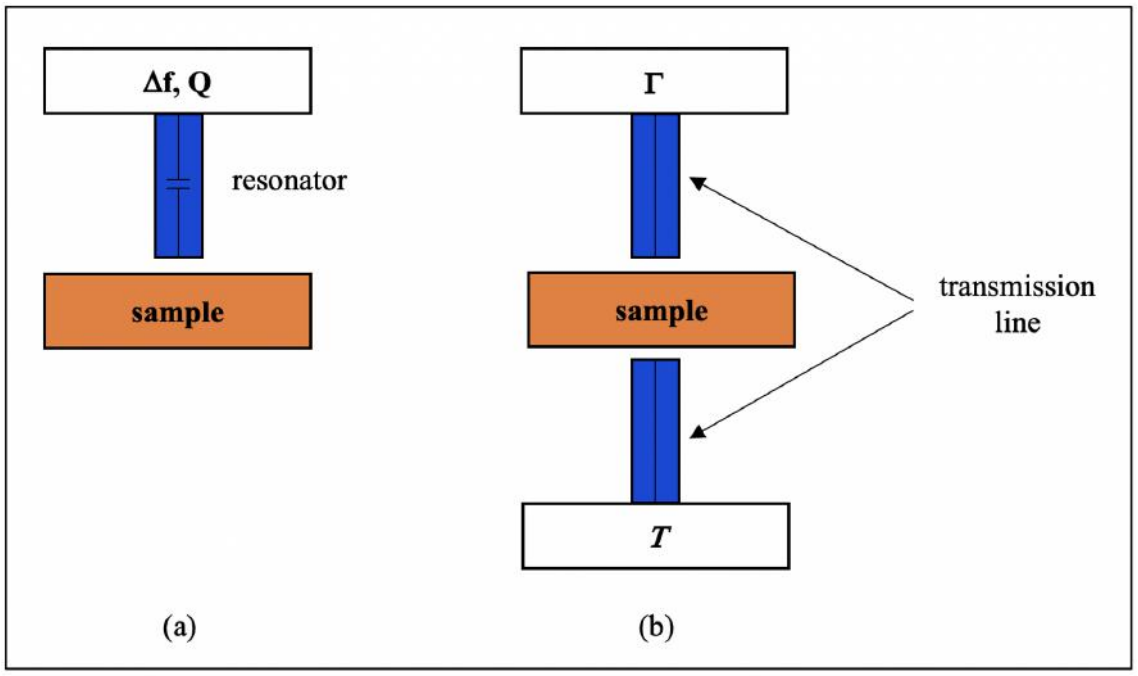

Figure 1.8: The basic schematic diagrams of (a) resonant and (b) broadband microwave microscopes

The NSMM is able to provide non-invasive and label-free imaging means for localized microwave characterization of the sample owing to the low microwave photons energy of a few tens microelectron-volts (μeV) that neither electronic structures nor chemical bonds will be disrupted. Ergo, this technique has gained interest in various application fields including biology. Recent studies have shown that the this technique is not only capable of examining the structure of biological cells [12], but also in measuring and quantifying the dielectric constant of lipid bilayer [13], the electric permittivity of single bacterial cells [14], and the complex impedance of CHO cells and E. coli [15].

However, thus far the NSMM application in the biology field is still limited to dried samples as the NSMM probe tip is incompatible with the physiological buffer. This is because the physiological buffer has higher dielectric permittivity than that of the air causes the parasitic interaction between the entire probe body and conducting sample holder become worse thus reduce the sensitivity. An advanced in understanding the intracellular biology is still dictated by the development of new scanning techniques allowing to study of both morphology and physiology of the living cell.

State-of-the-art

One of the commercial SMM is developed by Keysight Technologies (Santa Rosa, USA). It interfaces the VNA operating between 1 and 20 GHz with the AFM as shown in Figure 1.9 (a) [16]. Figure 1.9 (b) shows the Keysight SMM standard setup [17]. In the setup, an impedance matching network consists of $l/2$ resonator and 50 ω shunt resistor, inserted between the VNA and the AFM probe to match the impedance system of the probe so that the it is sensitive to detect very small changes in the sample impedance.

Another SMM system is produced by PrimeNano Inc. with a commercial name of Scanning Microwave Impedance Microscopy (SMIM). The instrument is composed of the high sensitivity of signature electronics design and the customized shielded AFM probe. The SMIM allows direct access to the conductivity and permittivity of the sample as it is based on the capacitive coupling between the sample and the AFM probe. Besides, it able to perform real-time detection of the capacitive and the resistive characteristics separately. The SMIM instrument is operated only at a single frequency of 3 GHz. Figure 1.10 shows the basic schematic diagram of SMIM [18].

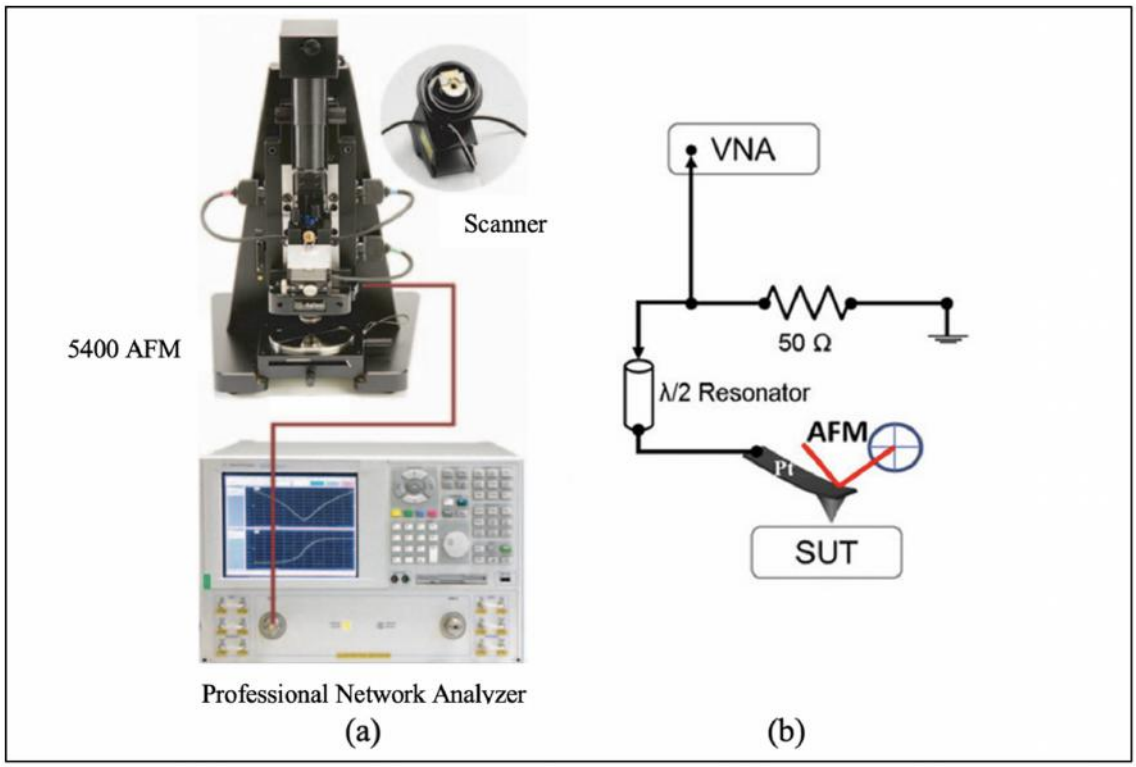

Figure 1.9: (a) The Keysight SMM and (b) the Keysight SMM standard setup

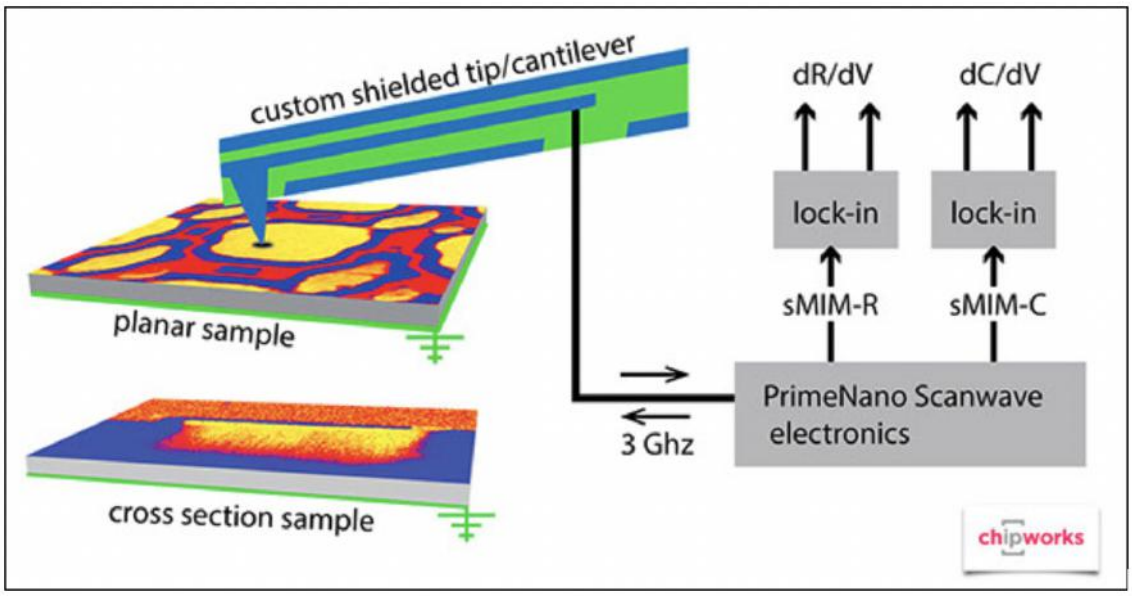

Figure 1.10: The SMIM basic schematic diagram

Chapter 2

Inverted Scanning Microwave Microscopy

2.1 Introduction

The near-field Inverted Scanning Microwave Microscopy (iSMM) is a new scanning microwave technique, recently developed by Farina et al. [19] on 2019 with the main objective to overcome the limitation addressed by the conventional SMM on sensitivity issue in biology application. They demonstrated the first successful microwave imaging of live cells in physiological conditions. Later, in the same year, this technique has applied to the inorganic materials, resulted in good sensitivity and quality of quantitative imaging [20]. The iSMM requires a slight modification of the SPM probe into a simple and rugged metal tip, and utilization of a transmission line such as slot line or coplanar waveguide as part of the sample holder. In both cases, the AFM-modified iSMM and the slotline have been used on live L6 cells and platinum diselenide ($PtSe_2$) respectively.

In contrast to the conventional SMM, the microwave signal in the iSMM setup is injected through the transmission line and the probe is always grounded. The microwave excitation and measurement are performed through the sample holder

whereas the probe is used as a perturbation tool to the sample. In such manner, the parasitic interaction is significantly reduced as most of the surround parts are grounded. As a result, the iSMM has higher sensitivity compared to the conventional SMM, forthright able to resolve the probe compatibility issue in physiological buffer. Figure 2.1 shows the schematic diagrams of the conventional AFM-based SMM and iSMM.

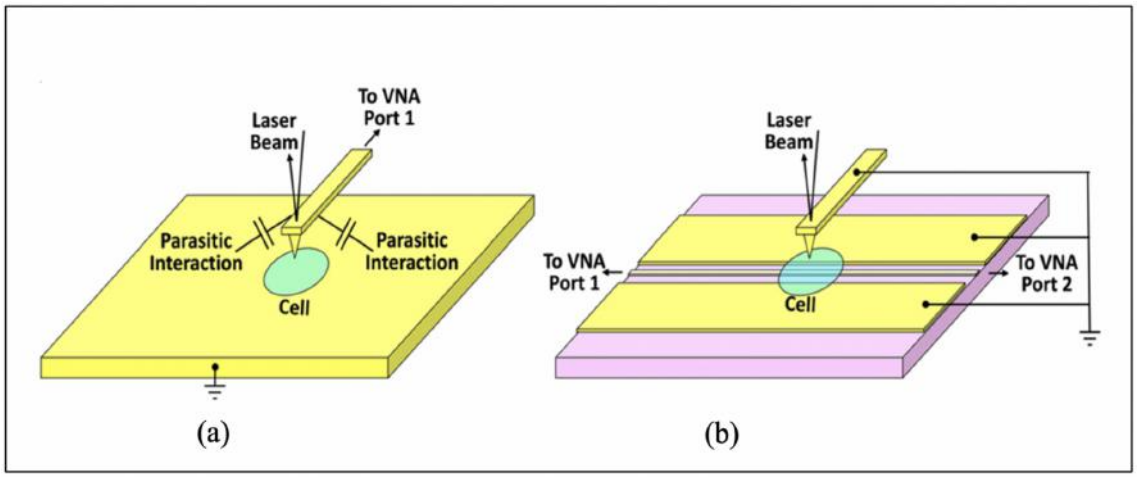

Figure 2.1: The schematic diagrams of (a) a conventional AFM-based SMM in one-port configuration and (b) an iSMM in two-port configuration [19]

Besides that, the input and output ports of the transmission line are connected to the VNA to allow the measurement of both reflection and transmission coefficients. With regards to the high SNR, the iSMM able to fully benefited from the wide dynamic range feature offered by the two-port configuration measurement that has been demonstrated in previous work [19] as shown in Figure 2.2 below.

The image quality of S_{21} displayed higher contrast and finer resolution than that of S_{11}. The dynamic in the transmission is typically higher than that in the reflection, causes it to be more sensitive to the small perturbation induced by the probe during the scanning process. Meanwhile, for the conventional SMM, the two-port configuration measurement is impractical as it does not contribute additional value but produce a faint replica image [21] [22].

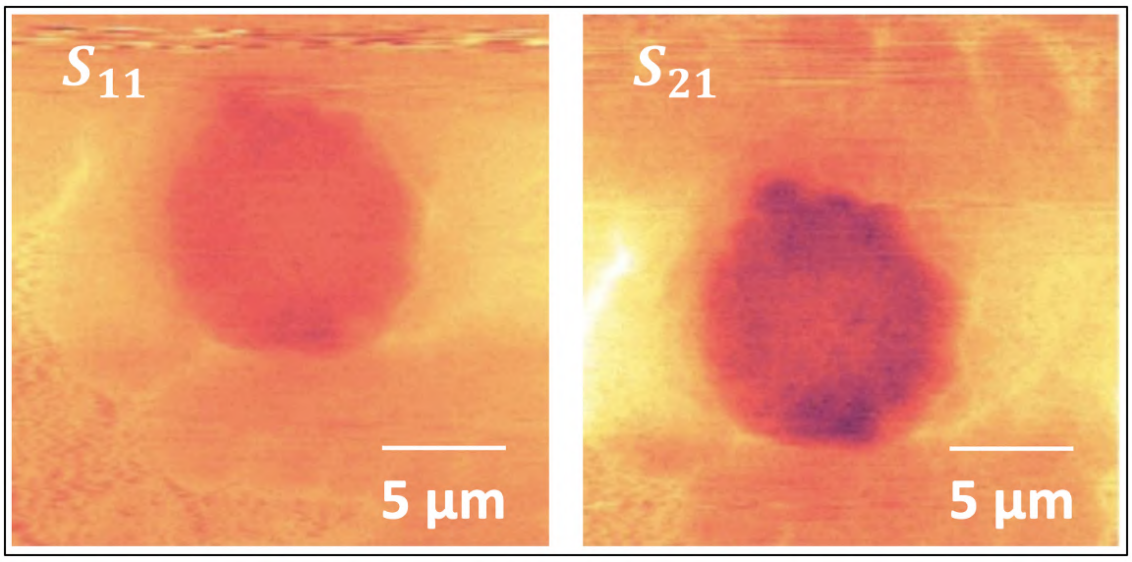

Figure 2.2: The iSMM images of dried L6 cell in air based on S_{11} and S_{21} respectively [19]

Furthermore, the iSMM sample holder allows either a fixed frequency or broadband measurement to be performed in the same setup. Apart from providing information at relevant frequencies and tomography, broadband microwave scanning enables the time-domain analysis in post-processing to further increase the image quality by filtering out the unwanted signals [23].

Albeit the aforementioned advantages of iSMM, the spatial resolution is determined by the tip dimensions and the SPM-based iSMM also allows the acquisition of high frequency microwave image together with a topography, similar to the conventional SMM. In summary, the iSMM provides better performance for microwave scanning and has open up opportunities to many applications beyond surface physics and semiconductor technology. However, further improvements are required to optimize the technique for future development.

Figure 2.3 shows the first iSMM prototype, the slot line sample holder that has fabricated in collaboration with Lehigh University (Pennsylvania, USA) by converting their commercial SMM into the iSMM.

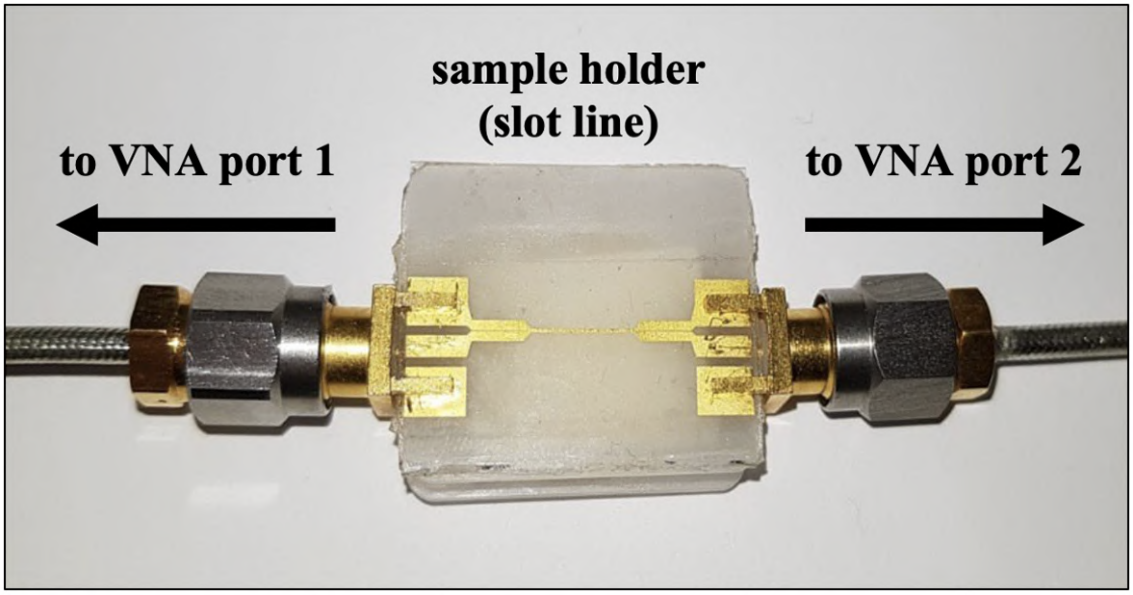

Figure 2.3: The iSMM first prototype

2.1.1 Transmission Line

Microwave imaging is performed in a frequency range varies typically from few gigahertz to few tens of gigahertz (GHz). Such high frequencies require a transmission line for the signal propagation along the desired path. In iSMM, the planar transmission line used to transmit the microwave signal to the sample subsequently to the VNA for the measurement that also served as a sample holder. It consists of conductive signal line placed on a dielectric substrate with precise geometry to ensure the signal propagates with minimum possible losses.

Slotline is a type of planar transmission line that was utilized in previous works [19] [20]. The structure composes of a narrow gap in the conductive coating on one side of the substrate surface. Coplanar waveguide (CPW) instead, has a center conductive strip, the signal line separated by narrow gaps from two parallel ground planes, equidistant from it, will be used in the present work. The purpose of the gap in both structures is to concentrate the field density between the conductor strips allowing to transmit the microwave signal efficiently. Figure 2.4 shows the schematic of both planar transmission lines.

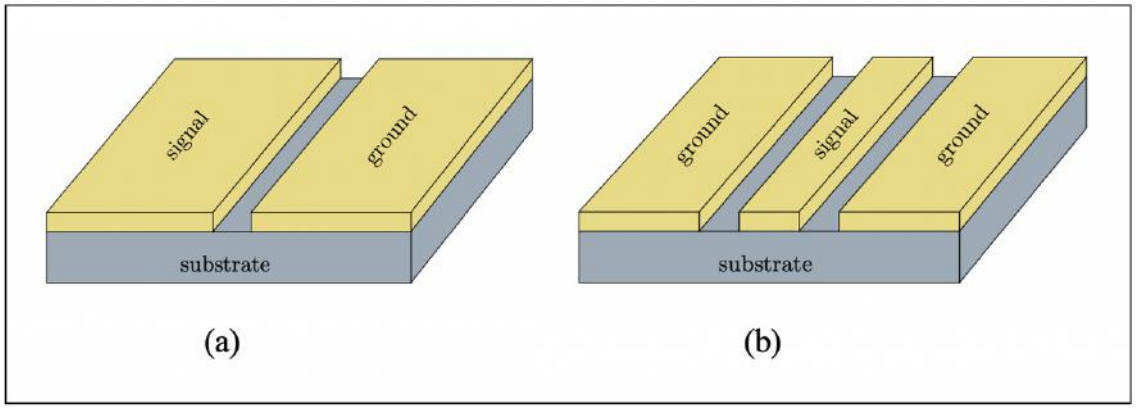

Figure 2.4: (a) The slotline and (b) coplanar waveguide (CPW)

2.2 Calibration Procedure

The microwave calibration procedure allows to quantitatively characterize the intrinsic sample properties. It requires a set of calibration sample with known loads called the standards, that is used to determine the unknown variables in the measurement and the unwanted interactions coming from the surrounding will be eventually removed.

The calibration technique demonstrated by Karassi et al. [24] and Huber et al. [25] employed an array of known capacitive loads as the standards. The replacement of the sample under analysis with the calibration sample encounters the differences in parasitic interactions between both measurements, mainly due to the presence of the interaction with the sample holder.

Then, in-situ calibration technique has been developed [26] [22] to improve the measurement accuracy by removing the undesired effects coming from the cables, connectors, geometry of the tip-sample interaction area and surrounding part of the microscope. In this technique, the unknown measurement of these effects are embodied in the one-port error network model of the sample admittance being measured, refer Figure 2.5 (a). The model requires at least three measurements of known loads, the standards that are the capacitance at three different distances from a ground plane, over a frequency range as shown in the Figure 2.5 (b).

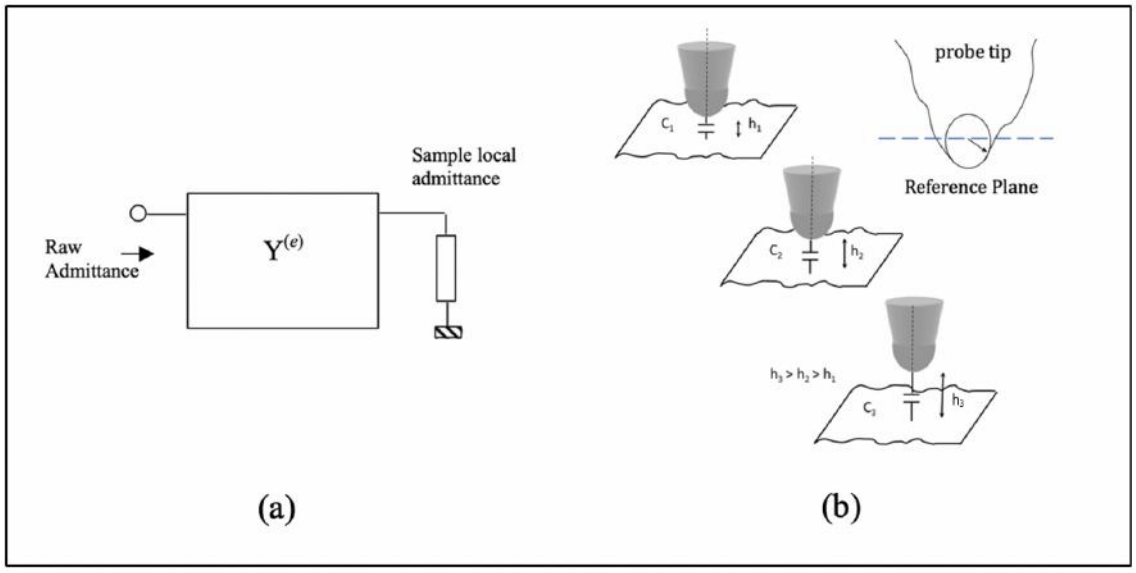

Figure 2.5: (a) The schematic of the calibration measurement and (b) definition of reference plane and three known loads measurement [22]

The reference plane is a critical element as it indicates what measurements will be considered in the error network. The reference plane defined at the probe tip allows removal of the undesired effects involving the cross-talk at the lateral part of the tip due to the topography effect.

In this work, this calibration technique is applied in order to get the local sample impedance.

2.3 Time Domain Analysis

Time domain analysis is a post-processing procedure that helps to filter out the unwanted signal from the image for higher SNR by performing inverse-Fourier transform on the reflection coefficient data over a given frequency range [23]. As the microwave image is composed of contributions from both near-field and far-field interactions, the description of the recorded reflection coefficient changes with time allows the possibility for the local and non-local signals to be partially disentangled. This is attributed to the fact that the local interactions at the tip apex are instantaneous while the non-local interactions are delayed by a certain period of time. On

top of that, despite this procedure take a great deal of time to process especially over wider frequency range, the reflection coefficient in time is a real quantity. It combines the informative data that might be hidden either in amplitude or phase (real or imaginary) plot during frequency sweeping and sometimes disseminate between the two. Therefore, the microwave image in the time domain displays higher quality compared to the frequency domain. The contribution of the time domain analysis can be visualized in Figure 2.6 of breast cancer cells MCF-7 (dried) [27].

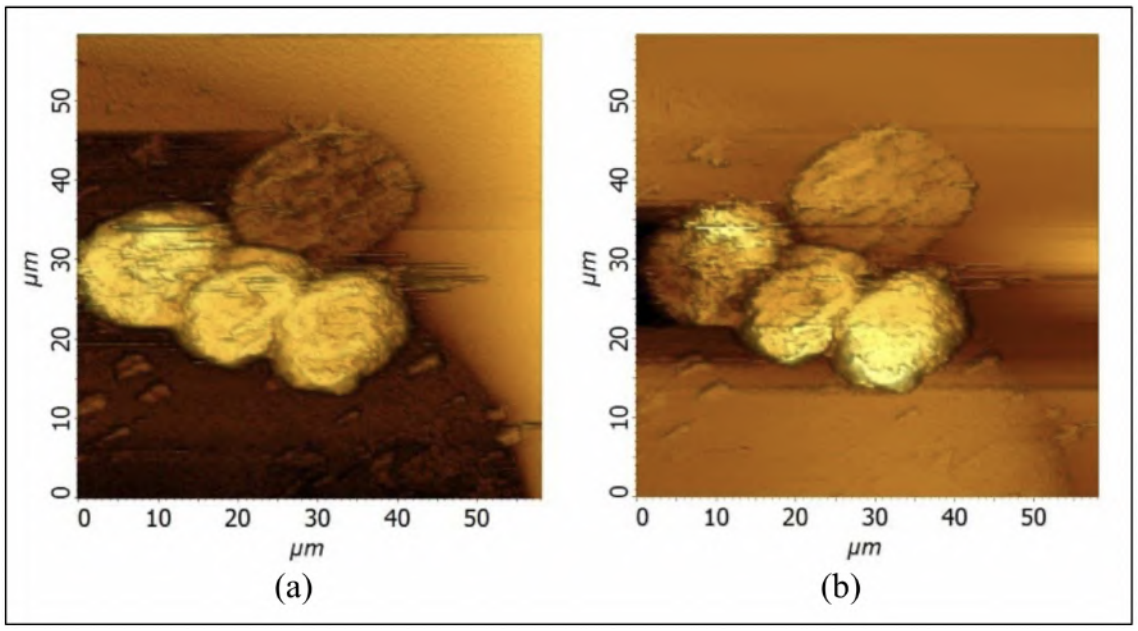

Figure 2.6: (a) The STM-based SMM image (corrected) and (b) the same image after the time-domain analysis, revealing the details of the image that was not visible in the STM image

Chapter 3

Experiment, Results and Discussion

3.1 Sample Preparation

Graphene has been used as the sample for this iSMM study and was prepared by exfoliating a highly oriented pyrolytic graphite (HOPG) flat surface substrate of $1.0 \times 1.0 \times 0.02 cm$ in 10 mL dimethylformamide (DMF) solvent through a sonication procedure. The graphene was sonicated for two hours resulting in multiple layer sheets. The dispersed graphene of 20 µL was then deposited on the CPW and let dried for few hours to be ready to get analyzed by AFM-modified iSMM as shown in Figure 3.1.

Figure 3.1: The exfoliated graphite

3.2 Experimental Setup

Figure 3.2 shows the iSMM setup that composed of the NT-MDT Solver Pro-47 AFM and the CPW from Signal Microwave. The CPW center signal line was terminated with SMA connectors at both ends that were then connected via coaxial cables to the two ports of the Keysight Technologies E8361A VNA operating between 10 MHz and 67 GHz. Both the reflection and transmission coefficients are measured by the VNA. The AFM probe, a gold tip NSG03/Au TipsNano with the curvature radius of 35 nm is electrically grounded. The optical microscope was used to facilitate in properly align the focused laser beam on the AFM cantilever.

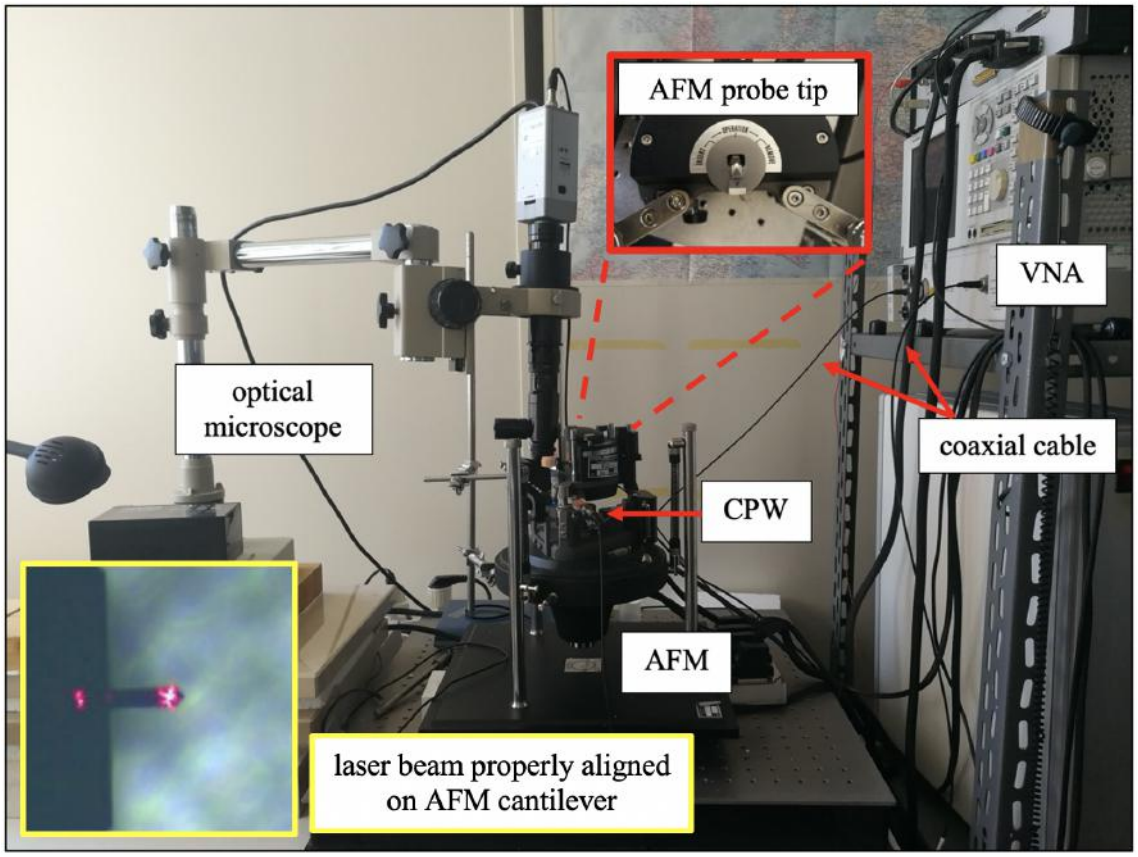

Figure 3.2: The iSMM setup

3.3 System Sensitivity

Before performing broadband microwave scanning, the sensitivity of the AFM-modified iSMM setup was evaluated to understand the overall system performance by monitoring the S-parameters of the VNA. Figure 3.3 shows the two-port configuration measurement obtained over the operating frequency of the VNA, between 10 MHz and 67 GHz.

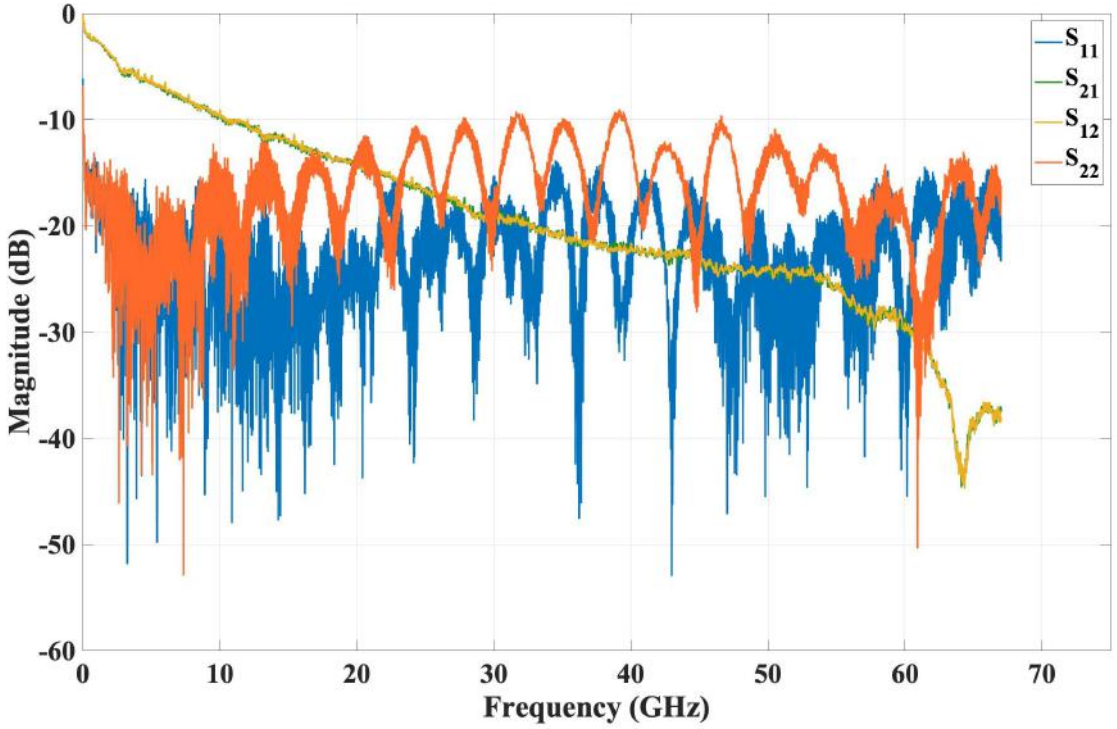

Figure 3.3: The S-parameter of iSMM setup

Based on the measurement, the system was considered asymmetric and reciprocal as $S_{11} \neq S_{22}$ and $S_{21} = S_{12}$, respectively. The resonances generated in the S_{11} were different from in the S_{22}, indicating the mismatch of the circuit at both input and output ports that caused by the physical implementation of the microwave signal paths connected between the VNA and the transmission line. Meanwhile, the S_{21} and S_{12} displayed consistence decay over the frequency range correlates to the power dissipation principle in which the higher the frequency, the higher the power dissipated. Therefore, the overall AFM-modified iSMM system performance

was reasonable and acceptable for microwave scanning.

3.4 Waveguide Analysis

After that, the CPW performance was measured to understand the behavior and to ensure no excessive signal distortion takes place. Two different analyses were done that are the analysis across and along the CPW signal line involving one-port and two-port configuration measurements over frequency range of 1 to 5 GHz.

3.4.1 Sensitivity Analysis Across Signal Line

In the one-port configuration, the CPW was connected to the port 1 of the VNA and terminated with 50 Ω at the other end. The measurement of the SNR of S_{11} was recorded at five different positions sequentially from Gap 1 to Gap 2 across the signal line as shown in Figure 3.4.

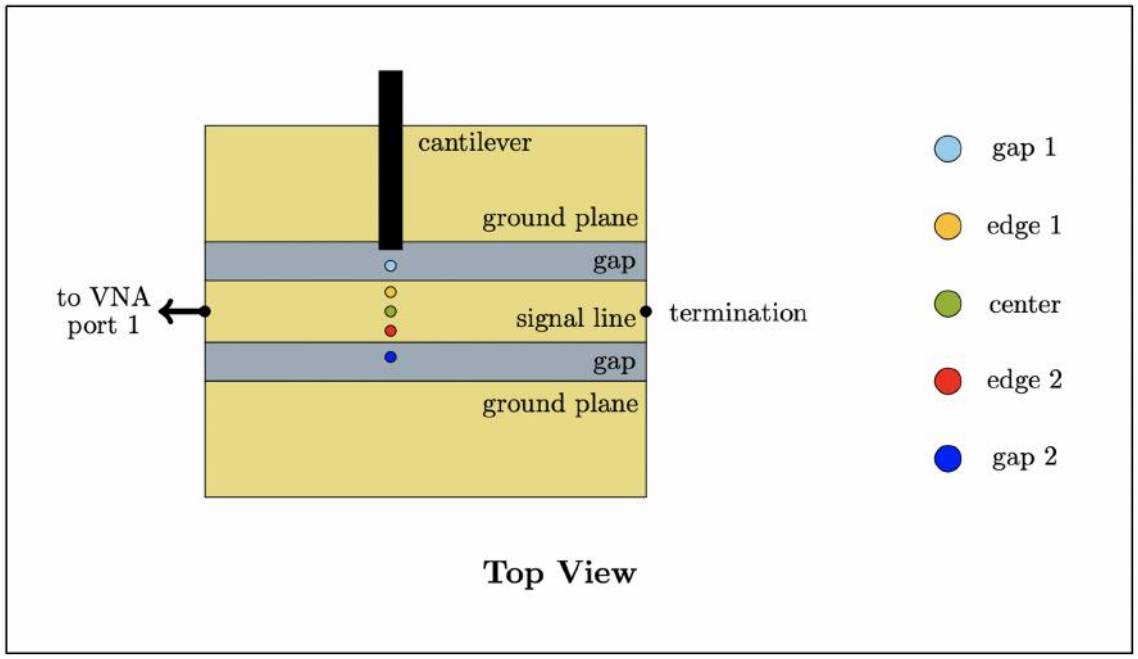

Figure 3.4: The five different positions across the CPW for SNR measurement of S_{11}

Figure 3.5 illustrates the SNR measurement of S_{11} obtained for all the mentioned

positions. The graphs showed a downward trend between 1 and 3.5 GHz and then remained stable at a higher frequency.

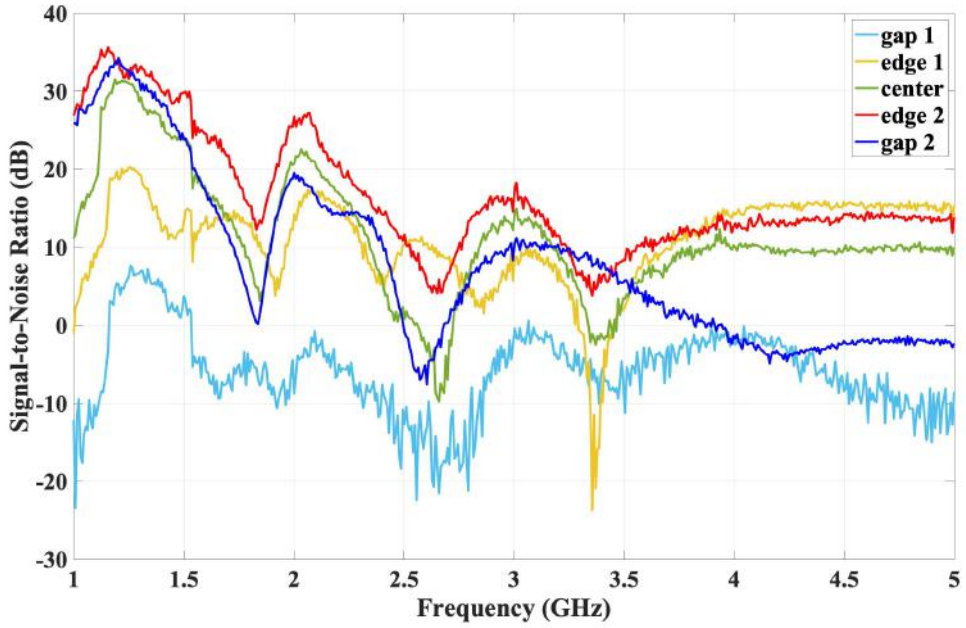

Figure 3.5: The SNR measurement of S_{11} graphs across the CPW

A fixed frequency, 1.16 GHz was selected for further discussion. Based on the histogram in Figure 3.6, the SNR measurement of S_{11} increased from the position of gap 1 to edge 2 and then slightly decreased at the gap 2 position.

The lowest SNR value at the gap 1 position is because the measurement was recorded out of the signal line, refer Figure 3.7 (a). As the cantilever moved forward across the signal line, the stray capacitance between the cantilever body and the signal line as shown in Figure 3.7 (b) caused the significant increased of the SNR value. Then, despite gap 2 position is out of the signal line, the SNR was still high due to the presence of the stray capacitance showed in Figure 3.7 (c).

3.4.2 Sensitivity Analysis Along Signal Line

In two-port configuration, the input and output ports of the CPW were connected to both ports of VNA. The measurement of the SNR of S_{21} was recorded at 3 different

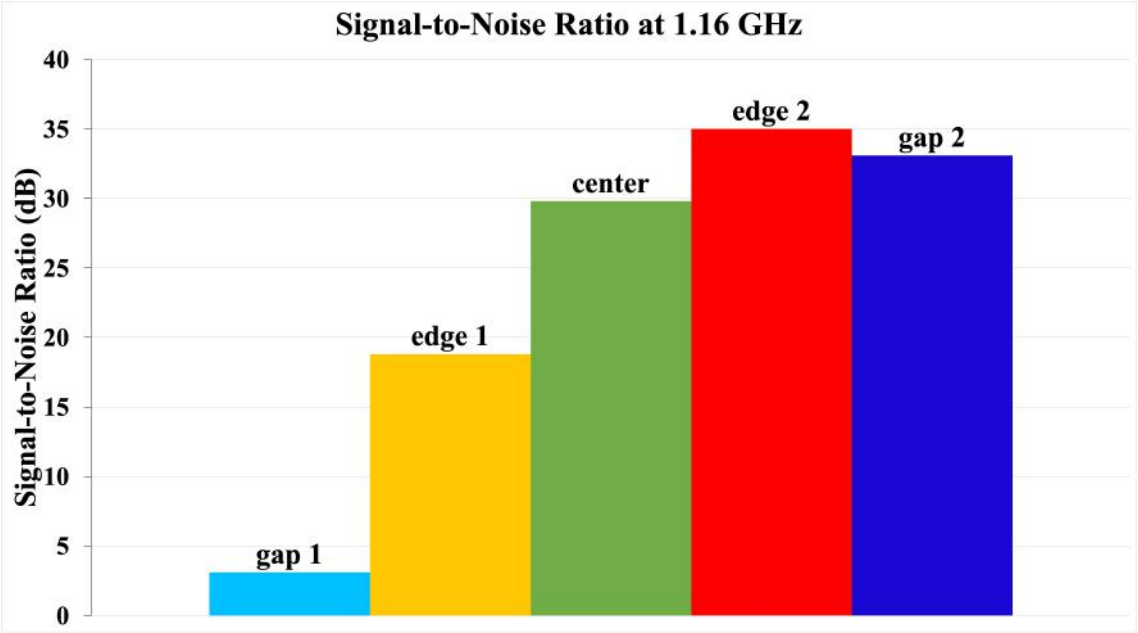

Figure 3.6: The SNR measurement of S_{11} at 1.16 GHz

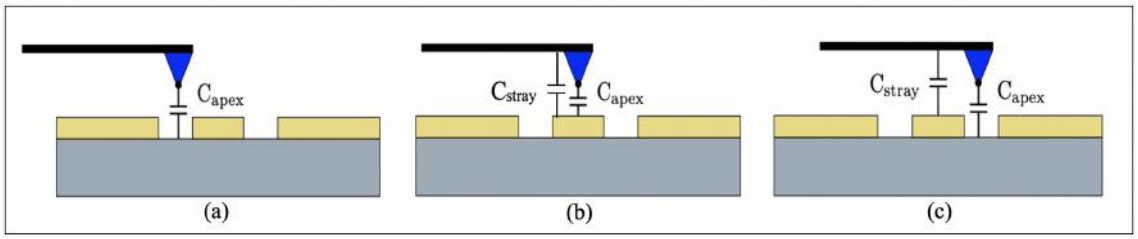

Figure 3.7: The capacitance coupling between the AFM cantilever and the CPW

positions along the signal line as shown in Figure 3.8. Point 1 position was located at the center of the CPW. Following with point 2 and point 3 positions towards one end of the CPW that was connected to the port 2 of VNA.

Figure 3.9 illustrates the SNR measurement of S_{21} obtained for the three different positions and similar to the analysis across the CPW signal line, the graphs in Figure 3.9 showed a downward trend between 1 and 3.5 GHz and remained stable at a higher frequency.

Based on the analysis of SNR measurement of S_{21} at 1.3 GHz in the Figure 3.10, the point 1 position provided the highest SNR value and was decreasing towards the end of the CPW. The SNR value changes along the signal line because the field is position-dependent and it has wavelength comparable with the size of the

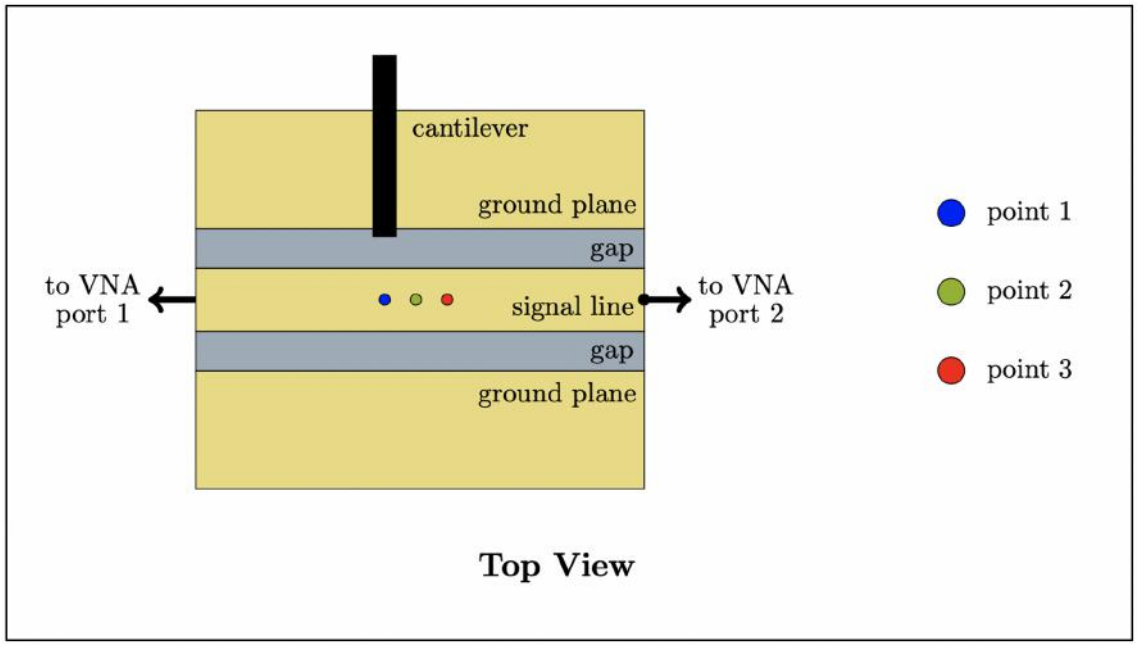

Figure 3.8: The three different positions along the CPW for SNR measurement of S_{21}

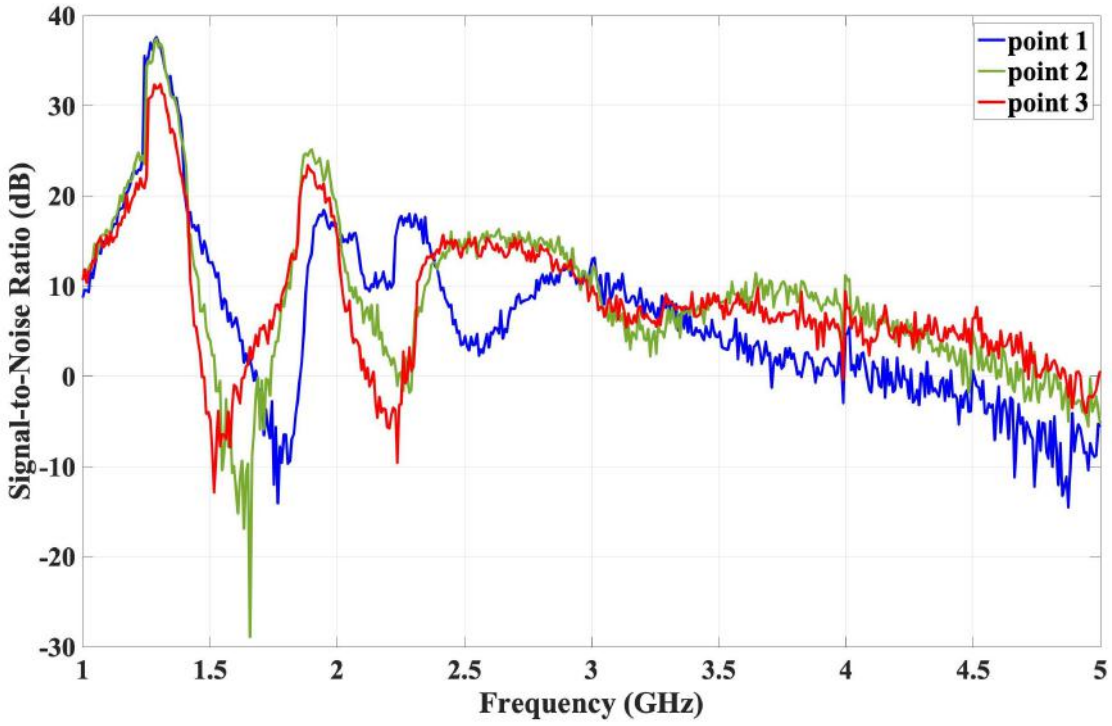

Figure 3.9: The SNR measurement of S_{21} graphs along the CPW

waveguide. Hence, changes of frequency along the line, will cause the sensitivity to change.

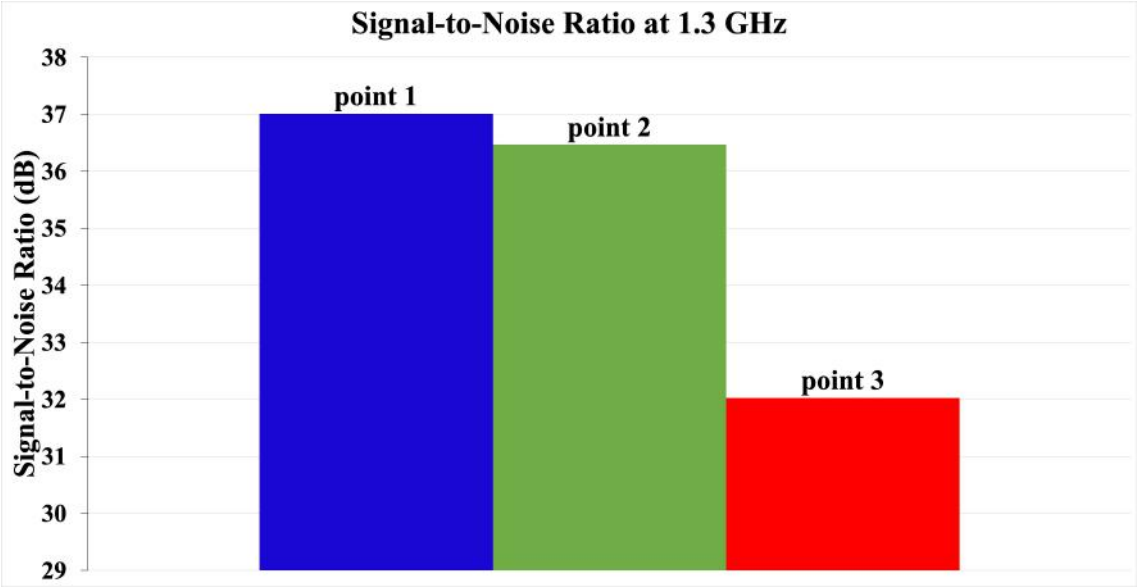

Figure 3.10: The SNR measurement of S_{21} at 1.3 GHz

In summary, the CPW behaves as expected and the optimal area for the sample to be deposited was at the center of the signal line in order to have high sensitivity thus obtain a good microwave image quality.

3.5 Sensitivity Test

Next, the operating frequency range for AFM-modified iSMM was identified because the system works in broadband wherein the resonator was not present to provide high sensitivity. For this reason, the sensitivity test of the system was performed. Within this frequency range, the unwanted contributions signal will be minimum resulting good quality either in magnitude or phase of microwave image. The sensitivity can be evaluated as follows

$$SNR(p(f)) = 20log\left(\frac{p1(f) - p2(f)}{\sigma(p(f))}\right) \tag{3.1}$$

where $p(f)$ is either the magnitude or phase of the microwave reflection coefficient $S11$, $p1(f)$ and $p2(f)$ are the $p(f)$ measured under two distinct conditions of probe-tip configuration such that with and without the feedback, corresponding to

a change in distance of $1 - 1.5\mu$m. The measurement was repeated for 500 times for each condition and averaged, so do for the standard deviation $\sigma(p)$. Generally, the optimal operating frequency band is selected with high $SNR > 20$ dB for plotting good frequency-domain microwave images quality. Figure 3.11 below shows the selected operating frequency range between 12.02 – 12.04 GHz of reflection coefficient, S_{11} that provided high SNR up to 23 dB. This frequency range was applied to produce the microwave images.

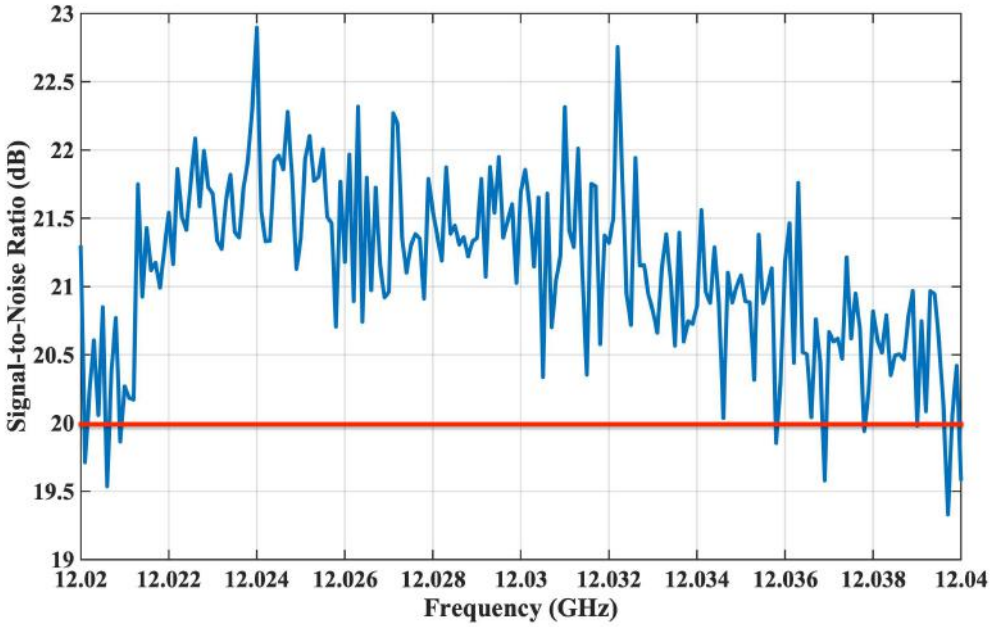

Figure 3.11: The operating frequency range for the iSMM

3.6 Results and Discussion

The graphene or graphite has been chosen as a sample to be analyzed to verify the performance of the developed AFM-modified iSMM tool.

The AFM-modified iSMM measurement was performed for one-port configuration and the image was produced from variations in the reflection coefficient, S_{11}. Figure 3.12 shows the AFM topography and iSMM image of graphite flake for a scan area of $5.0 \times 5.0um^2$ in 256×256 pixels acquired simultaneously. It can be

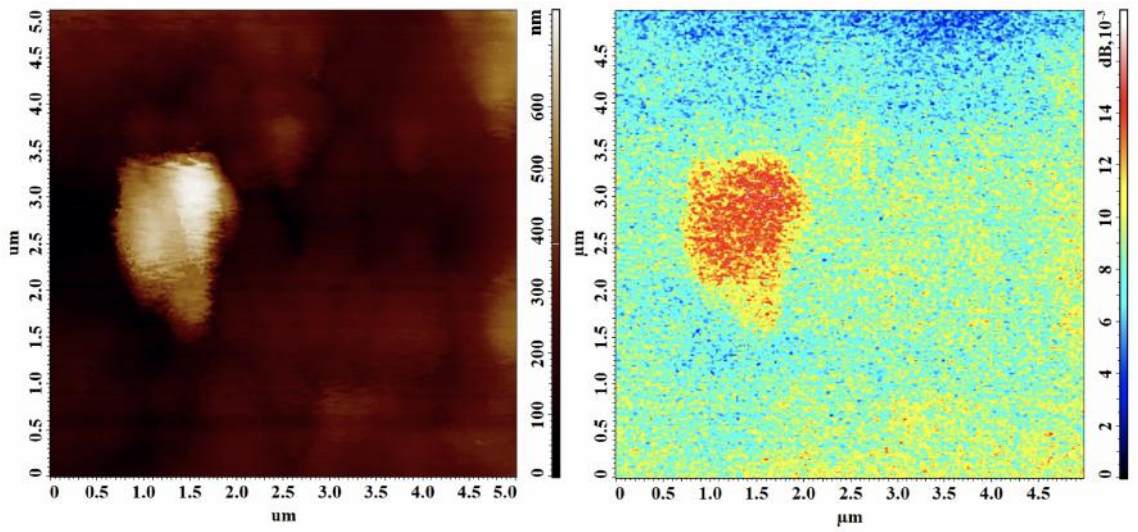

(a) AFM image (b) iSMM image

Figure 3.12: The simultaneous AFM and iSMM images of the graphite flake. The iSMM image is based on the magnitude of the reflection coefficient at 12.03 GHz.

seen that the quality of the iSMM image obtained is comparable to the AFM image. Figure 3.13 shows the graphite height profile is about 600 nm.

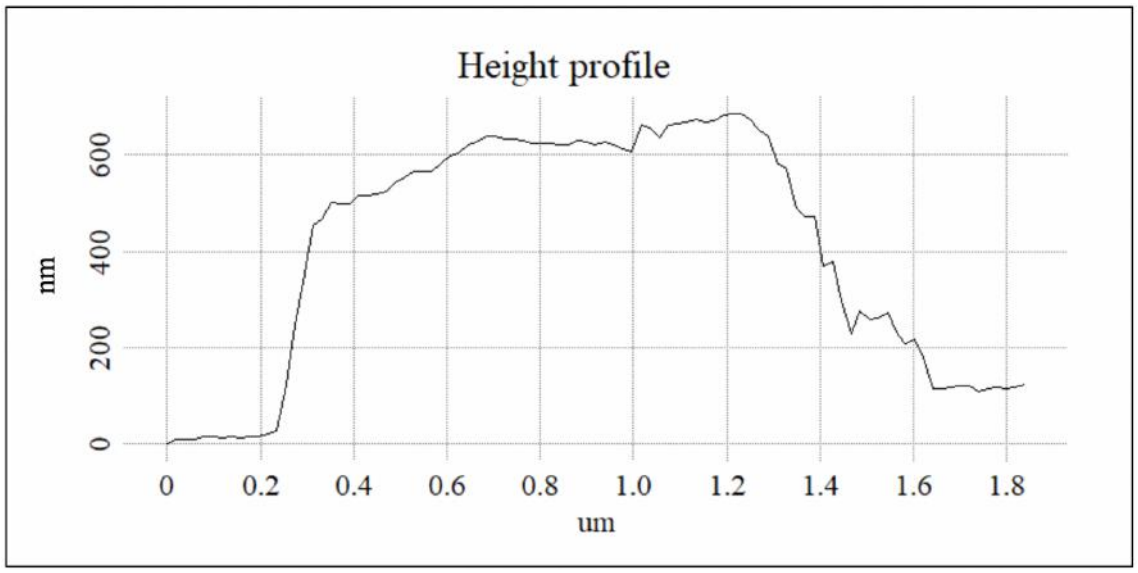

Figure 3.13: Graphite height profile acquired from AFM

The reflection coefficient, S_{11} was calibrated with the tip at different distances of 100, 500 and 1000 nm from the metal ground plane of the CPW sample holder. The tip was approximating as a sphere with a radius of 100 nm [22]. Figure 3.14

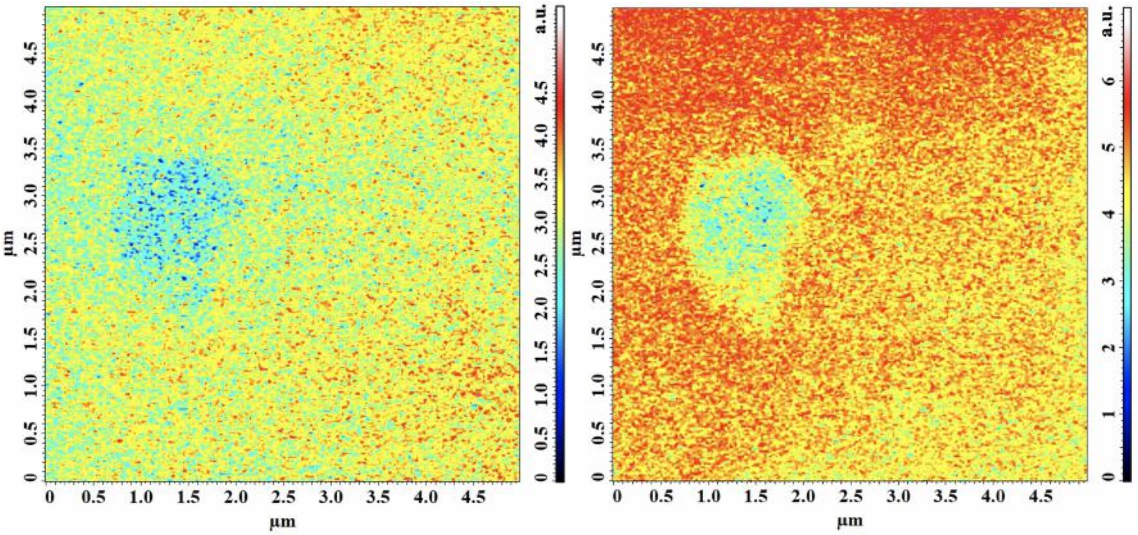

(a) Real part (b) Imaginary part

Figure 3.14: The calibrated iSMM images of graphite flake for both real and imaginary parts at 12.03 GHz

presents the calibrated iSMM images for both real and imaginary parts.

After the frequency domain calibration of the obtained S_{11} image, the time domain analysis was performed by inverse Fourier transform which disentangle the unwanted tip-microscope interaction for further improvement of the microwave image [23]. Figure 3.15 shows the time domain graphite flake image with better quality and revealing the details of the image that was not visible in AFM image.

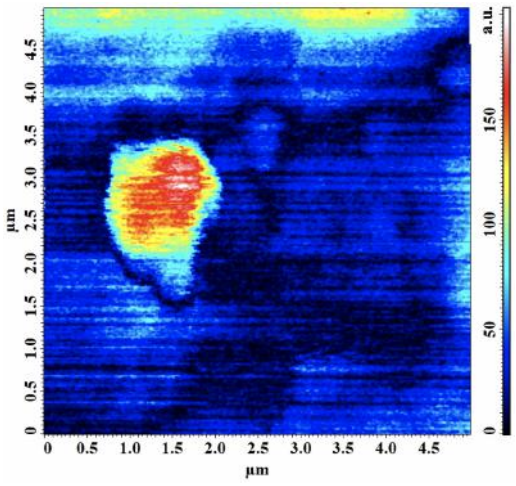

Figure 3.15: The iSMM in time domain image of graphite flake

Summary

The AFM-iSMM based on CPW transmission line has been developed and its capability in performing high frequency imaging of graphite flake is demonstrated. The developed iSMM shows better sensitivity when the tip cantilever is placed at the center of the signal line of the CPW. Both the AFM and iSMM images are showing good sensitivity and quality. The calibration procedure has been applied to raw S_{11} image at 12.03 GHz obtained by the iSMM, removing all the stray effects coming from the cables, connectors, geometry of the tip-sample interaction area and surrounding part of the microscope. The calibrated S_{11} image provided for both real and imaginary parts corresponding to the graphite flakes local admittance. The time domain analysis applied to the obtained frequency domain calibrated S_{11} image which combine the real and imaginary part thus displays higher S_{11} image quality. As a conclusion, the AFM-modified iSMM has been successfully developed and demonstrated effectively to image graphite flake at high frequencies.

Bibliography

[1] V Iglesias, M Porti, M Nafría, X Aymerich, P Dudek, and G Bersuker. Dielectric breakdown in polycrystalline hafnium oxide gate dielectrics investigated by conductive atomic force microscopy. *Journal of Vacuum Science & Technology B, Nanotechnology and Microelectronics: Materials, Processing, Measurement, and Phenomena*, 29(1):01AB02, 2011.

[2] Michael A Walsh and Mark C Hersam. Atomic-scale templates patterned by ultrahigh vacuum scanning tunneling microscopy on silicon. *Annual review of physical chemistry*, 60:193–216, 2009.

[3] Silvia Hormeno, Marcos Penedo, Cristina V Manzano, and Mónica Luna. Gold nanoparticle coated silicon tips for kelvin probe force microscopy in air. *Nanotechnology*, 24(39):395701, 2013.

[4] Reza Saber, Saeed Sarkar, Pooria Gill, Behzad Nazari, and Faramarz Faridani. High resolution imaging of igg and igm molecules by scanning tunneling microscopy in air condition. *Scientia Iranica*, 18(6):1643–1646, 2011.

[5] Arvind Raman, S Trigueros, A Cartagena, APZ Stevenson, M Susilo, E Nauman, and S Antoranz Contera. Mapping nanomechanical properties of live cells using multi-harmonic atomic force microscopy. *Nature nanotechnology*, 6(12):809–814, 2011.

[6] Ryo Yamada and Kohei Uosaki. In situ, real time monitoring of the self-assembly process of decanethiol on au (111) in liquid phase. a scanning tunneling microscopy investigation. *Langmuir*, 13(20):5218–5221, 1997.

[7] Gerd Binnig, Heinrich Rohrer, Ch Gerber, and Edmund Weibel. Surface studies by scanning tunneling microscopy. *Physical review letters*, 49(1):57, 1982.

[8] Gerd Binnig, Calvin F Quate, and Ch Gerber. Atomic force microscope. *Physical review letters*, 56(9):930, 1986.

[9] Gerd Binnig and Heinrich Rohrer. Scanning tunneling microscopy. *Surface science*, 126(1-3):236–244, 1983.

[10] M Born and E Wolf. Principles of optics, 6th corr. ed. *Cambridge University Press, Cambridge*, 33:52, 1998.

[11] Steven M Anlage, Vladimir V Talanov, and Andrew R Schwartz. Principles of near-field microwave microscopy. In *Scanning probe microscopy*, pages 215–253. Springer, 2007.

[12] Marco Farina, Andrea Di Donato, Tamara Monti, Tiziana Pietrangelo, Tatiana Da Ros, Antonio Turco, Giuseppe Venanzoni, and Antonio Morini. Tomographic effects of near-field microwave microscopy in the investigation of muscle cells interacting with multi-walled carbon nanotubes. *Applied physics letters*, 101(20):203101, 2012.

[13] Georg Gramse, Aurora Dols-Pérez, MA Edwards, Laura Fumagalli, and G Gomila. Nanoscale measurement of the dielectric constant of supported lipid bilayers in aqueous solutions with electrostatic force microscopy. *Biophysical journal*, 104(6):1257–1262, 2013.

[14] Maria Chiara Biagi, Rene Fabregas, Georg Gramse, Marc Van Der Hofstadt, Antonio Juaérez, Ferry Kienberger, Laura Fumagalli, and Gabriel Gomila.

Nanoscale electric permittivity of single bacterial cells at gigahertz frequencies by scanning microwave microscopy. *ACS nano*, 10(1):280–288, 2016.

[15] Silviu-Sorin Tuca, Giorgio Badino, Georg Gramse, Enrico Brinciotti, Manuel Kasper, Yoo Jin Oh, Rong Zhu, Christian Rankl, Peter Hinterdorfer, and Ferry Kienberger. Calibrated complex impedance of cho cells and e. coli bacteria at ghz frequencies using scanning microwave microscopy. *Nanotechnology*, 27(13):135702, 2016.

[16] Wenhai Han. Introduction to scanning microwave microscopy mode.

[17] Silviu-Sorin Tuca, Manuel Kasper, Ferry Kienberger, and Georg Gramse. Interferometer scanning microwave microscopy: Performance evaluation. *IEEE Transactions on Nanotechnology*, PP:1–1, 08 2017.

[18] Benedict Drevniok. Smim sheds new light on what's inside technology.

[19] Marco Farina, Xin Jin, Gianluca Fabi, Eleonora Pavoni, Andrea Di Donato, Davide Mencarelli, Antonio Morini, Francesco Piacenza, Richard Al Hadi, Yan Zhao, et al. Inverted scanning microwave microscope for in vitro imaging and characterization of biological cells. *Applied Physics Letters*, 114(9):093703, 2019.

[20] Gianluca Fabi, Xin Jin, James CM Hwang, CH Joseph, Eleonora Pavoni, Lei Li, Kuanchen Xiong, Yaqing Ning, Davide Mencarelli, Andrea di Donato, et al. Inverted scanning microwave microscopy for nanometer-scale imaging and characterization of platinum diselenide. In *2019 IEEE MTT-S International Microwave Symposium (IMS)*, pages 1115–1117. IEEE, 2019.

[21] Lu Zheng, Di Wu, Xiaoyu Wu, and Keji Lai. Visualization of surface-acoustic-wave potential by transmission-mode microwave impedance microscopy. *Physical Review Applied*, 9(6):061002, 2018.

[22] Marco Farina, Davide Mencarelli, Andrea Di Donato, Giuseppe Venanzoni, and Antonio Morini. Calibration protocol for broadband near-field microwave microscopy. *IEEE Transactions on Microwave Theory and Techniques*, 59(10):2769–2776, 2011.

[23] Marco Farina, Agnese Lucesoli, Tiziana Pietrangelo, Andrea di Donato, Silvia Fabiani, Giuseppe Venanzoni, Davide Mencarelli, Tullio Rozzi, and Antonio Morini. Disentangling time in a near-field approach to scanning probe microscopy. *Nanoscale*, 3(9):3589–3593, 2011.

[24] A Karbassi, D Ruf, AD Bettermann, CA Paulson, Daniel W van der Weide, H Tanbakuchi, and R Stancliff. Quantitative scanning near-field microwave microscopy for thin film dielectric constant measurement. *Review of scientific instruments*, 79(9):094706, 2008.

[25] HP Huber, M Moertelmaier, TM Wallis, CJ Chiang, M Hochleitner, A Imtiaz, YJ Oh, K Schilcher, M Dieudonne, J Smoliner, et al. Calibrated nanoscale capacitance measurements using a scanning microwave microscope. *Review of Scientific Instruments*, 81(11):113701, 2010.

[26] G Gramse, M Kasper, L Fumagalli, G Gomila, P Hinterdorfer, and F Kienberger. Calibrated complex impedance and permittivity measurements with scanning microwave microscopy. *Nanotechnology*, 25(14):145703, 2014.

[27] M Farina, Francesco Piacenza, F De Angelis, D Mencarelli, A Morini, G Venanzoni, T Pietrangelo, M Malavolta, A Basso, M Provinciali, et al. Investigation of fullerene exposure of breast cancer cells by time-gated scanning microwave microscopy. *IEEE Transactions on Microwave Theory and Techniques*, 64(12):4823–4831, 2016.

[28] Y-M Lin, Christos Dimitrakopoulos, Keith A Jenkins, Damon B Farmer, H-Y Chiu, Alfred Grill, and Ph Avouris. 100-ghz transistors from wafer-scale epitaxial graphene. *Science*, 327(5966):662–662, 2010.